*instruments*

MDPI

*Article*

# A Broad Photon Energy Range Multi-Strip Imaging Array Based upon Single Crystal Diamond Schottky Photodiode

**Claudio Verona, Maurizio Angelone *, Marco Marinelli and Gianluca Verona-Rinati**

Industrial Engineering Department, Tor Vergata University of Rome, Via del Politecnico 1, 00133 Rome, Italy; claudio.verona@uniroma2.it (C.V.); marco.marinelli@uniroma2.it (M.M.); gianluca.verona.rinati@uniroma2.it (G.V.-R.)

* Correspondence: angelonemaurizio.it@gmail.com

**Abstract**

A multi-strip detector made of synthetic single crystal diamond (SCD), based on a p-type/intrinsic diamond/Schottky metal transverse configuration and operating at zero bias voltage, was developed for imaging from extreme UV (EUV) to soft X-rays. The photodetector was patterned with 32 strips made of boron-doped diamond directly deposited, by means of the CVD technique and the standard lithographic technique, on top of the HPHT diamond growth substrate. The width of each strip and the gap between two adjacent strips were 100 μm and 20 μm, respectively. The strips were embedded in intrinsic SCD of an active area of 3.2 × 2.5 $mm^2$, also deposited using the CVD technique in a separate growing machine. In the present structure, the prototype photodetector is suitable for 1D imaging. However, all the dimensions above can be varied depending on the applications. The use of p-type diamond strips represents an attempt to mitigate the photoelectron emission from metal contacts, a non-negligible problem under EUV irradiation. The detector was tested with UV radiation and soft X-rays. To test the photodetector as an imaging device, a headboard (XDAS-DH) and a signal processing board (XDAS-SP) were used as front-end electronics. A standard XDAS software was used to acquire the experimental data. The results of the tests and the detector's construction process are presented and discussed in the paper.

**Keywords:** multi-strip detector; SCD photodetector; imaging device; soft X-ray and UV; secondary electron emission



Academic Editor: Antonio Ereditato

Received: 22 September 2025
Revised: 18 October 2025
Accepted: 24 October 2025
Published: 28 October 2025

**Citation:** Verona, C.; Angelone, M.; Marinelli, M.; Verona-Rinati, G. A Broad Photon Energy Range Multi-Strip Imaging Array Based upon Single Crystal Diamond Schottky Photodiode. *Instruments* **2025**, *9*, 26. https://doi.org/10.3390/instruments9040026



## 1. Introduction

The detection of soft X-rays (SXRs) and extreme ultraviolet (EUV) radiation requires compact, visible-blind, solid-state detectors based on wide-band-gap materials. Applications such as in situ beam monitoring at synchrotron facilities, advanced photolithographic processes, astronomical and space observations, as well as tomography in magnetic-confinement nuclear-fusion reactors, demand position-sensitive photodetectors with high spatial resolution [1]. In addition, photodetectors must often operate under extreme conditions, including high temperatures and intense ionizing radiation environments. General requirements for photodetectors include a well-defined photon detection range, high sensitivity at the operating wavelengths, fast temporal response and a high signal-to-noise ratio [1].

Diamond, owing to its exceptional physical and electronic properties, fulfils nearly all these requirements. Its wide optical transparency (above 220 nm) makes it suitable for detecting photons from EUV to X-rays, enabling a broad range of scientific and technological

applications [2–4]. Furthermore, diamond-based photodetectors are compact, intrinsically visible-blind, highly radiation-hard and thermally robust, which makes them particularly attractive for operation in harsh environments [2,3].

Over the past 25 years, the availability of low-cost, high-pressure high-temperature (HPHT) single crystal diamond (SCD) substrates has boosted the development of chemical vapour deposition (CVD) techniques for the homoepitaxial growth of high-quality films, paving the way for advanced SCD-based photodetectors. Considerable effort has been devoted to improving synthetic diamond quality and device design. Various device geometries, such as metal–semiconductor–metal (MSM) and Schottky photodiodes, have been reported [4–6]. However, relatively few studies have addressed SCD-based imaging detectors [7–13], despite the fact that standard photolithography and metallization processes allow for the fabrication of high-resolution multi-strips or pixel devices.

Diamond photodetectors are typically fabricated with either planar interdigitated electrodes or transverse (sandwich-like) contacts. These configurations exhibit different detection characteristics, and the choice depends on the application. However, metal-contact devices are affected by secondary electron emission (SEE), which adds spurious current to the photon-induced signal, significantly altering the detector response [14]. Experimental studies [14,15] have shown that SEE strongly impacts UV and EUV detection, particularly in the 50–100 nm range, resulting in an additional current which can significantly contribute to the measured one. This additional current is unstable and can depend on the experimental set-up and environmental conditions (e.g., external electric fields, charging effects of the material surrounding the device, atmosphere pressure, etc.). This leads to poor reproducibility of the detector response, making a reliable absolute calibration difficult. While transverse devices can be shielded to suppress this effect, interdigitated structures require careful calibration to achieve accurate responsivity [15].

In recent years, multilayered SCD p-type/intrinsic/metal (PIM) Schottky photodiodes developed at the University of Rome Tor Vergata have demonstrated fast response times, excellent radiation hardness and high sensitivity to EUV and SXR radiation [16,17]. In these devices, heavily boron-doped diamond provides an ohmic contact [18], eliminating the need to remove the HPHT layer. Building on this approach, we aimed to develop a photodetector with imaging capability while avoiding SEE.

Here we present a prototype multi-strip photodetector fabricated from CVD-grown SCD at the University of Rome Tor Vergata. The device provides 1D imaging capability and is made without metallic electrodes: the strips are made of p-type diamond, a highly conductive but non-metallic material, patterned lithographically after CVD on HPHT substrates. This design suppresses secondary electron emission independently of device geometry, while preserving the excellent detection and imaging performance of diamond-based photodiodes.

Notably, other non-metallic multi-strip detectors have been reported in the literature, see, e.g., [5–10]. However, their primary goals were typically to enhance responsivity, improve low-energy photon transparency, or optimize sensitivity, rather than to specifically address secondary electron emission.

After this Introduction, in Section 2 the paper discusses the fabrication process of the new device, while in Section 3 the experimental characterization of the photodiode using UV and SXRs radiation is presented. Section 4 is a discussion of the reported results and, eventually, future development toward a 2D device is outlined.

## 2. Materials and Methods

### *2.1. Fabrication Method*

A prototype, synthetic multi-strip single crystal diamond photodetector based on a p-type/intrinsic diamond/Schottky metal transverse configuration, operating at zero bias voltage, was created and studied as an imaging detector in the photon range from EUV to soft X-rays. The device fabrication is based on a standard photolithographic technique and selective CVD growth of diamond films, employing a mask patterned on protective sacrificial Cr layers. The fabrication process consists of the following steps: (i) P-type diamond microstrip electrodes were selectively grown using a microwave plasma enhanced chemical vapour deposition (MWPECVD) technique on a commercial HPHT single crystal diamond substrate, by using a Cr plasma-resistant coplanar mask (200 nm thick) patterned using the photolithography technique. (ii) Then, the chromium mask was removed by wet etching (see steps 1 to 3 in Figure 1). Several prototypes with different strip widths (range 70–100 μm) and distance between two strips (range 10–30 μm) were created. In this work, the dimensions of each strip of the used photodetector were 3 mm length, 100 μm width and gap between two strips: 20 μm. (iii) To complete the fabrication procedure, on the already produced device (see step 4–5 in Figure 1), an intrinsic homoepitaxial diamond layer (about 1 μm thick) was selectively grown using the MWPECVD technique, which buried all the p-type diamond strips by means of a patterned Cr layer. Cr deposition was realized via the lift-off method. Lift-off in microstructuring technology is a method of creating structures (patterning) of a target material (e.g., Cr) on the surface of a substrate (e.g., diamond) using a sacrificial material (e.g., photoresist), see, e.g., [19]. Then, the intrinsic diamond was only deposited at sites which were not protected by the Cr. (iiii) Annealing in air was thus performed in order to remove the surface conductive layer of the as-grown intrinsic diamond film and, eventually, a semitransparent Pt electrode (10 nm thick) was thermally evaporated on the top surface of the intrinsic diamond layer, forming a Schottky junction with intrinsic diamond. The total sensitive region was $3.2 \times 2.5\ mm^2$. Patterned silver pads were deposited by evaporation on the p-type diamond strips to form an ohmic contact.

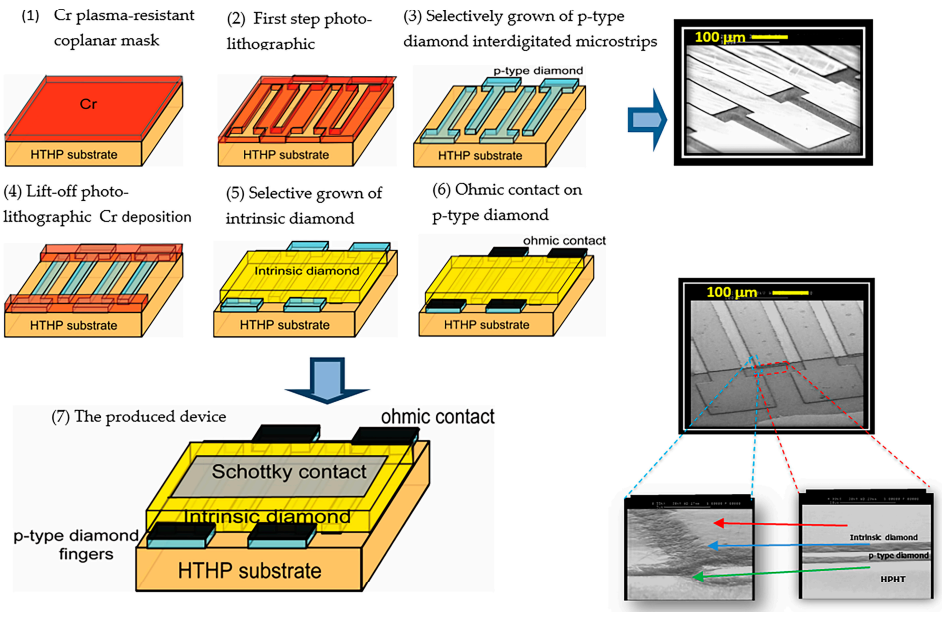


**Figure 1.** Scheme of fabrication process of the microstrip diamond device (picture from 1 to 6). Picture 7 shows the as-realized device. On the right side, four SEM pictures (in black and white) show details of the device: the two SEM figures on the top show details of the ohmic contacts of the strips, the two smaller SEM pictures on the bottom show details of the morphological structure of the photodetector.

The produced photodetector is shown in step 7 of Figure 1. Some details of the device are shown in the four SEM pictures of the device, reported on the right side of Figure 1.

Figure 2, in turn, shows further details of the photodiode, with emphasis on the electrical connections. Figure 2 is a vertical section of the device showing the single p-type diamond strips (grey rectangles with numbers) buried in the 1 μm thick intrinsic CVD layer. The latter is covered by a semitransparent Pt layer forming a Schottky contact with the intrinsic diamond. Since this metal contact is directly illuminated by the photons to be detected, it is grounded to eliminate secondary electron emission [15]. Owing to the presence of the Schottky contact, the device can work without the need of an external bias. For a Pt contact the Schottky built-in potential is about 2.1 V [20]. An external bias can be applied to the device, it is used to enhance the responsivity, as discussed in Section 3.1. The current signal is directly extracted from each strip, as discussed hereafter.

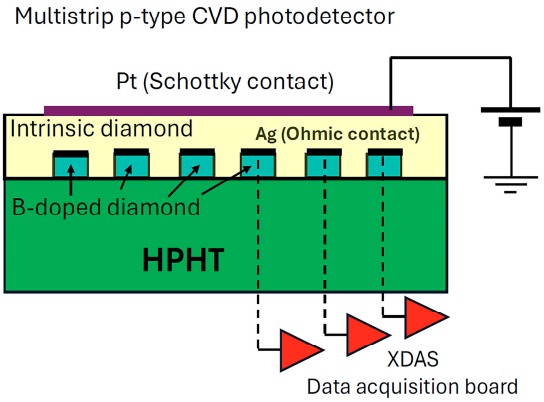


**Figure 2.** Vertical section of the photodiode, indicating the B-doped diamond strips and their ohmic contacts, achieved by evaporating Ag. The bias and electrical connections to XDAS acquisition board are also indicated.

The detector was then placed on a printed circuit board (PCB) connected to a commercial XDAS (Sens-Tech Ltd., Surrey, UK) data acquisition board (Figure 3a), made up of a detector board (XDAS-DH) and a signal processing board (XDAS-SP). Data interface to a PC was achieved via USB module, and a proprietary Sens-Tech Ltd. software was used for basic operation and data acquisition, respectively. Each one of the thirty-two strips was connected to an independent XDAS channel by micro-wire bonding, performed via ultra-sound technique using 25 μm diameter aluminum wire (see Figure 3b).

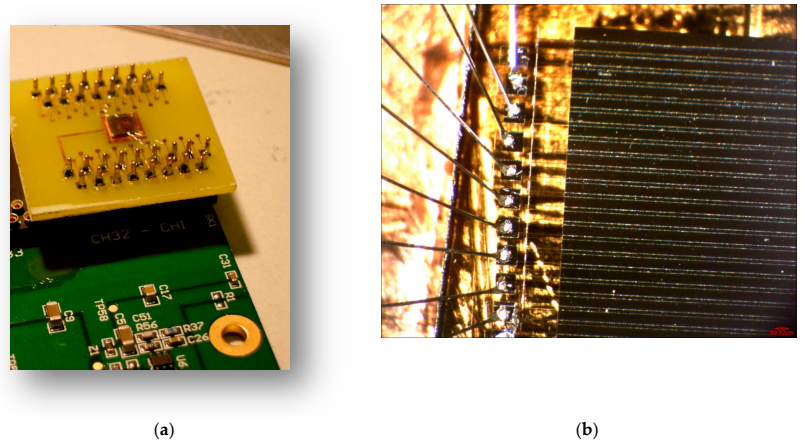

(**a**) (**b**)

**Figure 3.** (**a**) The detector mounted in the detector headboard (XDAS-DH), electrically connected to an ad hoc printed circuit board. (**b**) Detail of the electrical connections, which were achieved via micro-wire bonding using a 25 μm diameter aluminum wire.

### 2.2. Electrical Characterization

Once produced, the prototype photodetector was tested in order to study its electrical properties. Both dark current and capacitance were measured versus external bias voltage. The I-V curves were measured using a Keithley 6517A ammeter (Tektronix Ltd., Bracknell, UK), while the C-V characteristics were measured using an AGILENT 4263B LCR meter (Agilent, Santa Clara, CA, USA). In both cases, the single strip was connected to these instruments.

Figure 4a,b show the I-V and C-V curves measured for four strips selected among those with the larger differences in the measured dark current and capacitance. In both cases, data are plotted versus external bias voltage. It is worth noting the typical diode I-V curve in Figure 4a and the very flat C-V characteristics in Figure 4b.

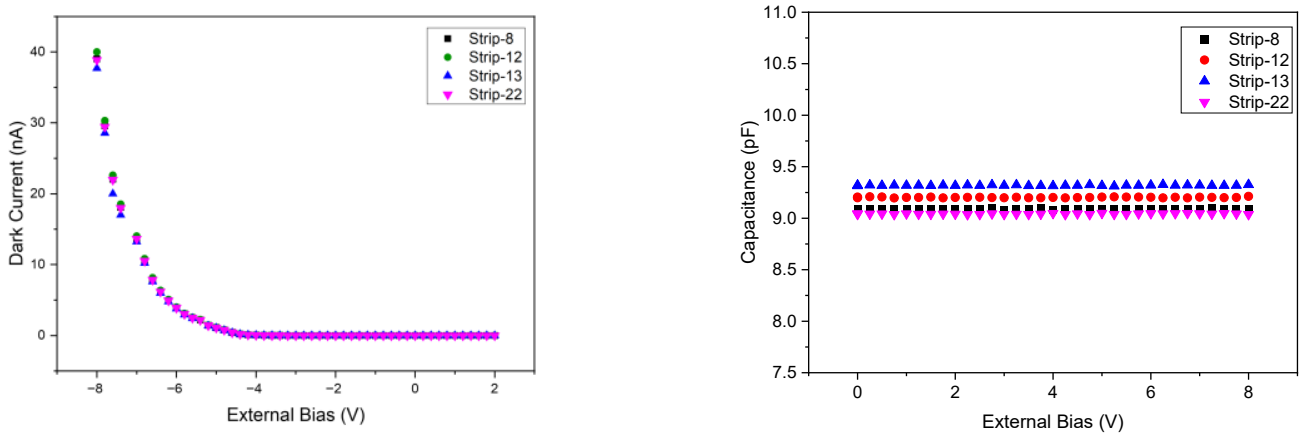


(**a**) (**b**)

**Figure 4.** (**a**) Measured I-V of four p-doped diamond strips, noting the typical diode response curve; (**b**) C-V characteristics measured for four strips. The results of the capacitance of the device are stable in the range of the studied external voltage bias.

The C-V curves were measured using twenty-five strips over the thirty-two total strips of the device; all the strips show very close results. The C-V data were used to determine the thickness W (in microns) of the intrinsic diamond layer, enveloping all the 32 p-type diamond strips. This was attained by assuming the detector to behave as a planar capacitor; thus, $W = \varepsilon_0 \varepsilon_1 A / C_{phd}$ where $\varepsilon_0$ and $\varepsilon_1$ are the dielectric constants for void and diamond ($\varepsilon_1$ = 5.7), respectively; A is the active area and $C_{phd}$ the capacitance of the device. The capacitance $C_J$ (in pF) of each one of the measured strips (J = 1, 2, ..., 25) was measured versus external bias voltage (see Figure 4b). Then, the capacitance $\langle C \rangle_J$ averaged over the external bias voltage range was calculated for the J-th strip. Thus, the photodiode capacitance $C_{phd}$ was defined as the average value over the measured nineteen strips: $C_{phd} = \Sigma_j(\langle C \rangle_J)/N$ (J = 1, 25). The standard deviation of the mean was calculated too. Figure 5 shows the results of the C-V measurements; each point corresponds to $\langle C \rangle_J$, and the averaged value $C_{phd}$ (red continuous line) and the standard deviation of the mean (blue dotted lines) are shown too. The small value of the standard deviation evidences the quality of the detector and the accuracy reached in the construction procedure. As far as the thickness W is concerned, a figure of W = (1.30 ± 0.05) μm was obtained, in good agreement with the 1 μm nominally deposited intrinsic layer thickness.

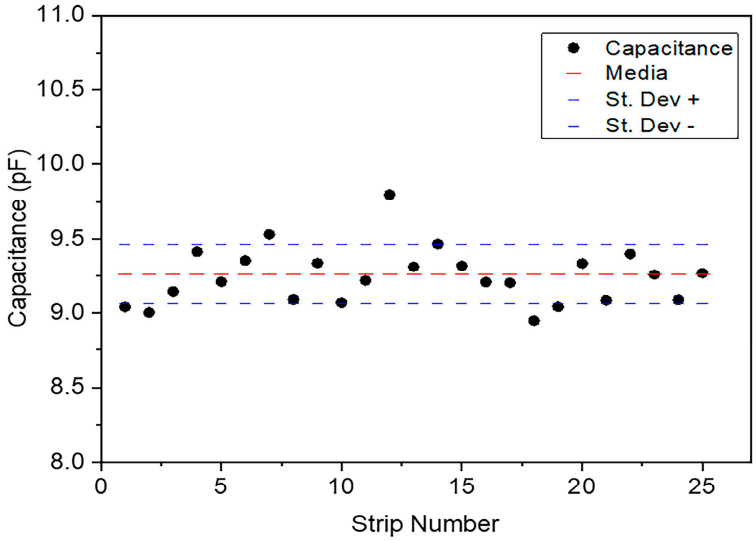


**Figure 5.** Measured capacitance of twenty-five over thirty-two strips. Each black point is the averaged value of the capacitance measured versus the external bias voltage using a single strip (see Figure 4b). The red line is the averaged capacitance over the twenty-five measured strips and the two blue dotted lines indicate the standard deviation of the mean.

### *2.3. Experimental Set-Up*

An extensive characterization of the device in terms of its imaging capabilities, the linearity of the response and the time response was performed by means of soft X-rays (SXR) and UV radiation. The test with SXR was performed at the beam line B16 of Diamond Light Source (DLS) (Harwel Science and Innovation Campus, Oxfordshire, UK). DLS is a synchrotron-light facility located in the UK. The test with UV was performed at the Industrial Engineering laboratory of Tor Vergata University using a Laser (220 nm) and a He-Ne lamp (HORIBA Jobin Yvon Inc., Edison, NJ, USA), the latter coupled to a Jobin-Yvon monochromator (HORIBA Jobin Yvon Inc.) to select single spectral lines in the EUV range.

The beam line B16 of DLS [21] is a versatile facility designed to test optics, detectors and other instrumentation. It is installed on a bending magnet and can deliver white beam and monochromatic beams in a photon energy range of 4 keV to 20 keV. The irradiation set-up of B16 is shown in Figure 6a. A He-tube was used to reduce the attenuation of the extracted photon beam impinging on the sample to be studied. When the refractive lens was installed, since the photodetector was operating in air, to reduce the beam attenuation, the measurements were performed using a micro-focused beam operating at 10 keV. In addition, the refractive lens used optimized performance in the range of 10–15 keV. The SXR beam dimensions were accurately determined both in the horizontal (X) and vertical (Y) direction by using slits for both micro-focused and unfocused beams. The size of the micro-focused beam is shown in Figure 6b and the results were 2.6 μm and 3.2 μm for horizontal and vertical directions, respectively.

Imaging tests were first performed at Industrial Engineering Department of Tor Vergata University laboratory under 220 nm, 5 ns pulsed UV laser irradiation using an Optical Parametric Oscillator (OPO) tuneable laser (OPOTEK, Carlsbad, CA, USA), (see Figure 7a) and a UV He lamp coupled to a Jobin-Yvon monochromator (HORIBA Jobin Yvon Inc.), (see Figure 7b).

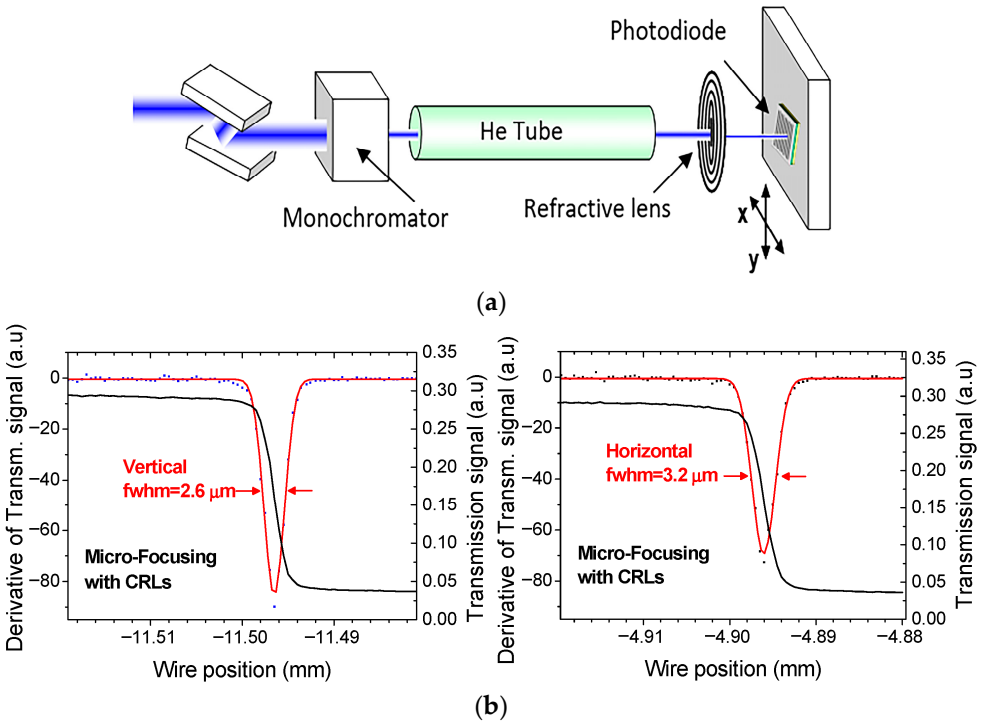


**Figure 6.** (**a**) Lay-out of the experimental set-up at the B16 beam line. With the photodiode located in air and the refractive lens installed and used to focus the beam, the measurements were performed using a micro-focused beam at 10 keV. (**b**) Vertical and horizontal measurements of the beam dimension for the micro-focused beam used during the measurements. The size of the micro-focused beam is given in the figure (FWHM) and the results were 2.6 μm and 3.2 μm for horizontal and vertical direction (X and Y axes in Figure 6a), respectively. The size of the micro-focused beam was measured by taking transmission scans of 200 μm diameter gold cross-wires. The derivatives of the gold wire scans gave the beam size.

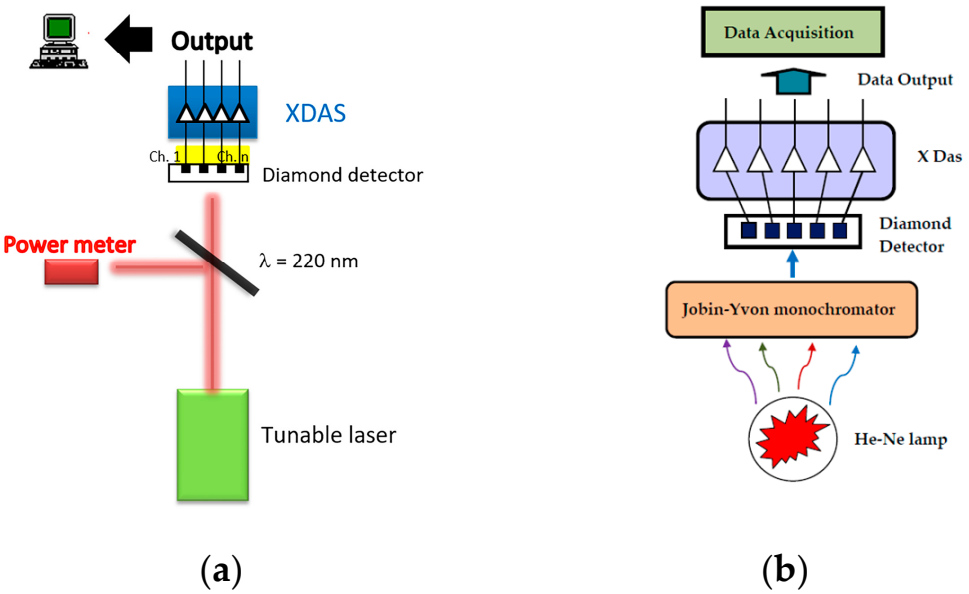


**Figure 7.** (**a**) Sketch of the experimental set-up used for the 220 nm UV (laser) measurements. (**b**) Sketch of the experimental set-up used for the He-Ne lamp coupled to Jobin-Yvon monochromator to select single spectral lines in the EUV range.

## 3. Results

### *3.1. Test of the Device with SXR*

The first test with SXR consisted of the study of the spatial resolution and response homogeneity of the photodiode by using an X-ray raster scan. The synchrotron was operating with a current of 200 mA in top-up mode. When the machine operates in top-up mode, a small amount of charge is injected every 10 min, allowing the current to stay constant, within ±1%, over the whole lasting time of the experimental test.

Once the micro-beam was focused on the device surface and its X-Y dimensions assessed (see Figure 6b), a detailed measure of the detector response was performed by scanning the whole surface of each strip. The current generated by the strips exposed to X-ray was read-out by means of Keythley 428 transimpedance amplifiers. The scanning pixel resolution was 3.2 μm × 2.6 μm. As already stated, the limited available beam time forced us to select a limited number of strips (only four). As an example of the results, Figure 8 shows a 3D map and a contour plot of four strips irradiated by 10 keV photons. Notably, there was excellent uniformity of the response over the scanned surface.

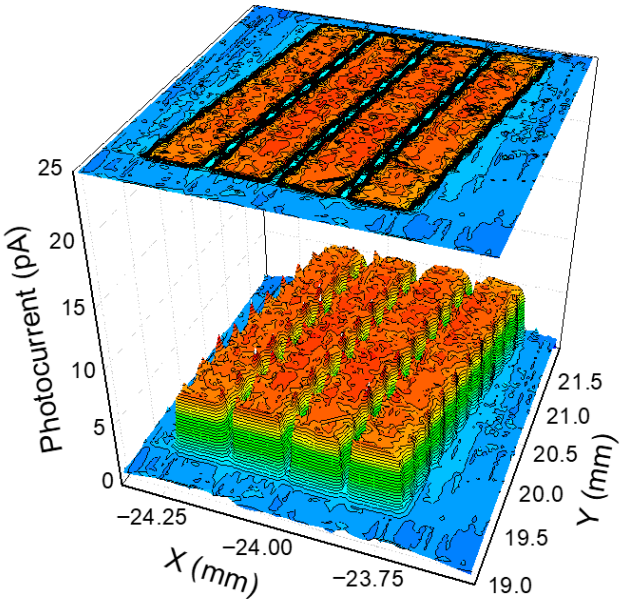


**Figure 8.** Contour plot (top) and 3D map (bottom) measured by four strips irradiated by using 10 keV X-ray and a pixel resolution of 3.2 μm × 2.6 μm. The plot reports the measured data as current (pA) because the voltage output of the transimpedance amplifier was converted to current using the amplification gain.

Figure 9 shows the profile of the photocurrent measured along the X direction for the same four strips discussed in Figure 8. The photocurrent was measured using three different external bias voltages. The bias is applied to each strip by means of an external circuit (see Figure 2). For each strip, the current profile is almost flat. However, two sharp peaks are observed at the edge of each strip. This is attributed to the presence of the gap between the two strips. The gap produces "vertical" edges, as shown in the two SEM pictures on the bottom of Figure 1. These gaps modify the detector's surface, which is no longer flat, thus affecting the homogeneity of the electrical field at the interfaces of two strips. The field gradient generated is thus responsible for the observed sharp peaks. Furthermore, no overlapping between pixel currents and a high discrimination between adjacent strips were observed. The application of external bias to the photodetector (from 0 to 4 V) results in an increase in the measured current. An value almost double that

of the measured current was observed at 4 V in the case of the unbiased detector. This result does not depend on the used strip (Figure 9).

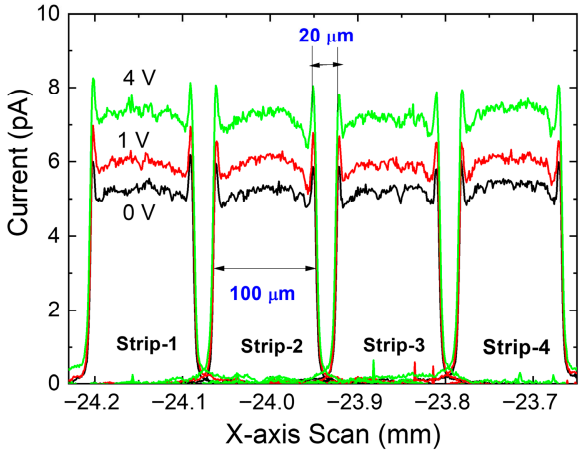


**Figure 9.** Horizontal scan, by mean of a raster scan, of four strips irradiated by 10 keV X-ray. The scanning pixel resolution was 3.2 μm × 2.6 μm. Two sharp peaks are clearly noticeable on both sides of each strip. These peaks are attributed to the electric field gradient generated by the discontinuity in the physical structure (gap between two strips) of the photodiode. As for Figure 8, the plot reports the measured data as current because the voltage output of the transimpedance amplifier was converted into current using the amplification gain. It is worth noting the increase in the measured current with the external bias voltage (1 V and 4 V, respectively).

### *3.2. Testing of the Device with UV*

To evaluate the UV response of the detector strips, the device was mounted on a horizontal translation stage and scanned with the laser beam. The 220 nm laser beam illuminates the entire active surface of the detector. This stage allowed for controlled movements of the detector along both left and right directions relative to the beam axis, with positioning managed by dedicated software. Each strip had a width of 100 μm with a 20 μm gap between adjacent strips, corresponding to a total scanned distance of about 1.9 mm in both directions. The purpose of this test was to investigate the detector's response when the detector was moved from "in-field" (centred on the beam) to "out-field" (displaced outside the beam). The results are summarized in Figure 10. When the laser was centred on the detector (Figure 10a), signals were observed on all twenty-five connected strips. The outermost strips, however, showed no response. Indeed, non-functioning outer strips (seven out of the thirty-two) were mainly due to excessive dark current and/or bonding issues with the external readout circuit. When the detector was shifted to the right of the beam axis (Figure 10b), or to the left (Figure 10c), the illumination profile changed accordingly, with the strips located near the displaced edge becoming inactive.

Pinholes with different diameters (0.25 mm, 0.50 mm and 1.0 mm) were also used in a new test to collimate the UV radiation and to change the size of the UV beam impinging on the sensitive area of the photodetector, with the goal of investigating its spatial resolution. The results for the three used pinholes are reported in Figure 11. As clearly shown, the effect of the pinhole diameter is to illuminate increasing portions of the active area of the photodetector. This is represented by the different numbers of black vertical bars (one bar indicates one strip) in Figure 11. The experimental data were fitted using a Gaussian function (red curves in Figure 11). For each used pinhole diameter, the FWHM (in μm) obtained from the Gaussian fit increases with the pinhole diameter, and its dimension is very close to the diameter of the used pinhole.

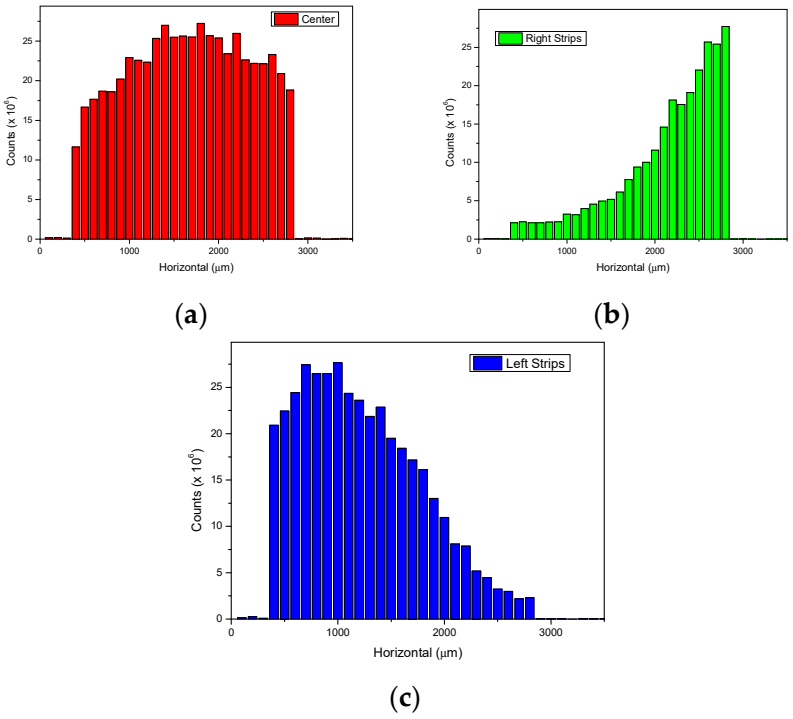


**Figure 10.** Response of the photodetector to the 220 nm UV laser beam. Each bar indicates one single strip; in total, there are twenty-five. The height of each vertical bar indicates the magnitude of the measured response of a single strip to UV laser photons. (**a**) Shows the results when the laser beam is centred with respect to the detector. All twenty-five strips are illuminated. (**b**) Shows the results measured when the photodiode is moved 1900 μm right. (**c**) Shows the results when the detector is shifted 1500 μm left with respect to the laser beam axis (see main text).

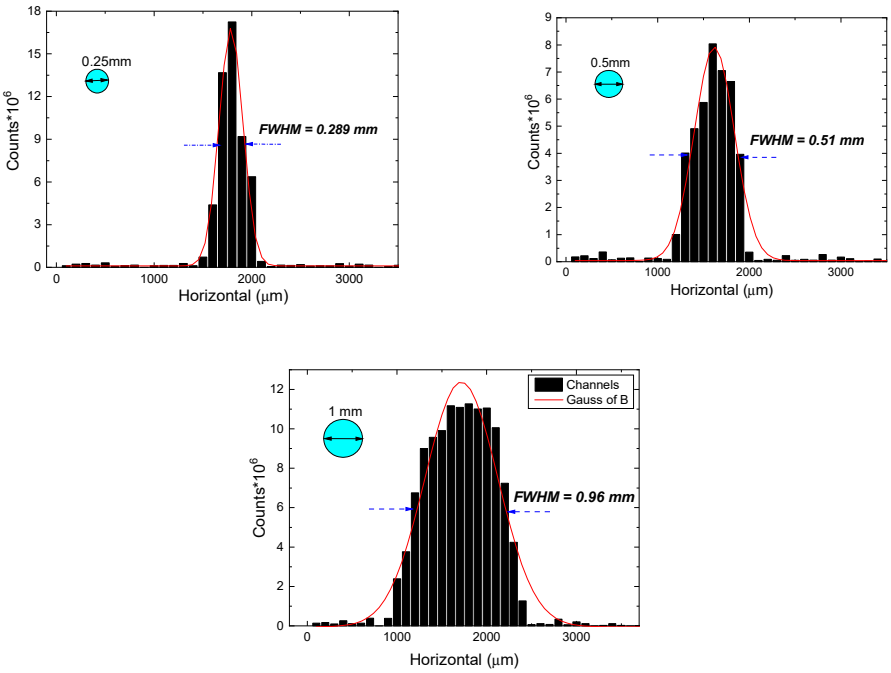


**Figure 11.** Spatial resolution test: measurement performed using three pinholes with different diameters: 0.25 mm, 0.5 m and 1 mm. The response depends upon the pinhole diameter. Each illuminated strip is represented by a vertical black bar whose height is proportional to the response of the single strip to the UV radiation. The red curves are the Gaussian fit to the experimental data; the calculated FWHM of each Gaussian curve is also shown.

Additional measurements were performed at different wavelengths, 30.4 nm and 58 nm, respectively, by using a UV He lamp and a Jobin-Yvon monochromator. The latter was used to select the different wavelengths. The results are shown in Figure 12. Again, the results demonstrated the excellent performances of the device. Also, in this case, all the measured FWHMs are compatible with the size of the used monochromator slit (250 μm–300 μm), as demonstrated in Figure 12a,b, where the Gaussian fit to the experimental data are shown together with the resulting FWHM. Furthermore, the results demonstrated that the detector responded over a wide range of wavelength, even if it responded with different efficiency (the vertical scale in Figure 12 is arbitrary but proportional to the signal amplitude produced by each strip).

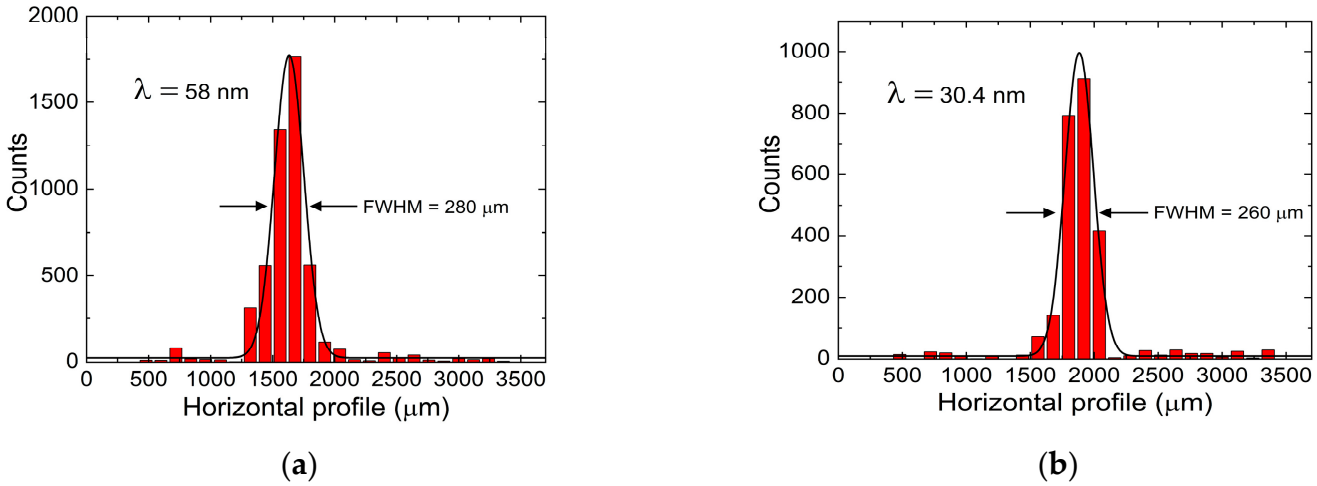


**Figure 12.** Response of the photodiode irradiated by a He-Ne lamp. Two monochromatic wavelengths were selected by a Jobin-Yvon monochromator: (**a**) λ = 58 nm and (**b**) λ = 30.4 nm. The vertical scale is arbitrary but proportional to the signal amplitude produced by each strip.

The linearity of the response versus photon flux impinging on the detector was measured for each strip, still using the He lamp without using the monochromator. As an example of the results, the response versus the plasma current of the He lamp is plotted in Figure 13.

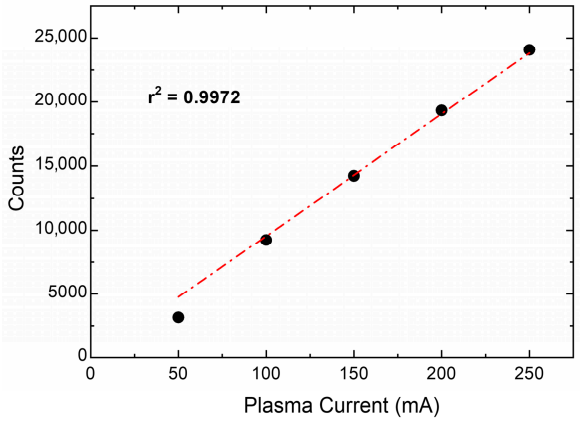


**Figure 13.** Measured linearity of one strip versus the plasma current of the He-Ne lamp.

## 4. Discussion

The results obtained using soft X-rays and UV radiation clearly point out the very good performances of the new diamond-based photodiode in terms of 1D imaging performances. All the requested features of a photodiode to be used for imaging are met. The use of

non-metallic strips seems not affect the properties of the new photodiode, rendering it comparable to photodiodes made with metallic contacts.

The construction procedure of the photodiode is based on a combination of photolithography and chemical vapour deposition of synthetic single crystal diamond techniques. By changing the number of strips, the spacing between strips and the thickness of the intrinsic active diamond layer during fabrication, different types of photodiodes can be produced in our laboratory, each with specific characteristics and performances. This was also performed (not reported in this work); other detectors were produced with strip pitch widths of 70 μm and 90 μm and with inter-strip distances of 4 μm and 10 μm. It was noted that the pitch width and the distance between two strips does not influence the presence of the sharp current peaks discussed in Figure 9. The results for detectors with different dimensions were always consistent with those discussed in this paper and demonstrated the good performances of these devices. Therefore, it ought to be stressed that only the detector discussed in this paper was tested at DLS with soft X-rays. The most limiting factor is still in the dimensions of the used HTHP diamond substrate, which usually has a side of 3 or 4.5 mm.

Since in the various produced detectors some of the strips were showing problems (e.g., high dark current and/or capacitance values) or were not working at all, improvement in terms of the fabrication technique is necessary. Possible causes of the mentioned problems could be related to the lift-off phase. It is known that there are three common disadvantages of this technique: (i) retention, that is, unwanted parts of the metal layer remaining on the wafer; (ii) formation of "ears" which occurs when the metal is deposited, and it covers the sidewalls of the resist; and (iii) redeposition. This last problem arises when particles of metal re-attach to the surface, at a random location. It is very difficult to remove these particles after the wafer has dried.

To solve or at least reduce these problems, it is necessary to improve the constructing procedure, which is presently conducted in our laboratory and in the future will require a customized procedure.

Despite the mentioned drawbacks, the excellent imaging properties shown above encourage further development of the device. One point to note is the 1D imaging performances, which can represent a limiting factor for the photodetector. To this end, a new version of the detector with enhanced 2D imaging capabilities is under study and design. The basic idea is to create a double-sided photodiode by also depositing the strips on the other face of the HTHP diamond substrate. The latter, which is usually 300 μm thick, must be properly reduced in thickness (e.g., to 20–30 μm) using reactive ion etching (RIE), in order to reduce the attenuation of the X-ray passing through the HTHP substrate. Secondly, the new p-doped diamond strips must be deposited at 90° with respect to those deposited on the first face of the HTHP substrate; in this way, a matrix-like structure will be obtained. This would allow for 2D capabilities. Of course, owing to the presence of the HTHP substrate, the detector is intended to be used with soft X-rays, whose range is dependent upon the HTHTP substrate thickness. Possible applications could be as an active X-ray beam monitor or as a compact detector in a tomography system.

## 5. Conclusions

A prototype of a single crystal diamond detector with buried p-type diamond strips, selectively grown on a commercial HPHT diamond substrate, has been developed to provide 1D spatial resolution in an effective horizontal dimension of 3.2 mm. This structure allows us to avoid spurious contribution from SEE emitted from the illuminated surface. These secondary electrons strongly affect the detection of extreme UV radiation and the prototype detector has been demonstrated to effectively solve the SEE problem. A new

detector with 2D imaging capabilities is under study, which could be proposed for use in X-ray detection. It is based on p-type diamond strips deposited on both sides of the HPHT substrate. The strips of one face must be deposited at 90° with respect to those of the other face, in order to form a matrix-like structure. The HPHT substrate, in turn, needs to be thin, e.g., 20–30 μm, so as to reduce X-ray attenuation.

**Author Contributions:** Conceptualization, C.V. and M.A.; methodology, C.V.; software, C.V. and G.V.-R.; validation, C.V., M.A., G.V.-R. and M.M.; investigation, C.V. and M.A.; data curation, C.V. and M.A.; writing—original draft preparation, M.A. and C.V.; writing—review and editing, G.V.-R., M.M., M.A. and C.V. All authors have read and agreed to the published version of the manuscript.

**Funding:** This research received no external funding.

**Data Availability Statement:** The data presented in this study are available on request from the corresponding author due to unavailability of public repository.

**Acknowledgments:** The authors wish to thank the staff of the beam line B16 for the warm hosting and the technical support during the experimental campaign.

**Conflicts of Interest:** The authors declare no conflicts of interest.

## References

1. Sang, L.; Liao, M.; Sumiya, M. A Comprehensive Review of Semiconductor Ultraviolet Photodetectors: From Thin Film to One-Dimensional Nanostructures. *Sensors* **2013**, *13*, 10482–10518. [CrossRef] [PubMed]
2. Angelone, M.; Bombarda, F.; Cesaroni, S.; Marinelli, M.; Raso, A.M.; Verona, C.; Verona-Rinati, G. X-ray and UV detection using synthetic crystal diamond. *Instruments* **2025**, *9*, 9. [CrossRef]
3. Koizumi, S.; Nebel, C.E.; Nesladek, M. (Eds.) *Physics and Application of CVD Diamond*; Wiley-VCH GmbH Co. KGaA: Wetnhetm, Germany, 2008; ISBN 978-3-527-40801-6.
4. Jia, L.; Zhu, S.; Zhang, N.; Lin, Z.; Cai, W.; Cheng, L.; Lu, X.; Zheng, W. Ultrafast Diamond Photodiodes for vacuum Ultraviolet Imaging in Space-Based Applications. *Adv. Opt. Mater.* **2025**, *13*, 2402601. [CrossRef]
5. Bloomer, C.; Newton, M.E.; Rehmb, G.; Salter, P.S. A single-crystal diamond X-ray pixel detector with embedded graphitic electrodes. *J. Synchrotron Rad.* **2020**, *27*, 599–607. [CrossRef] [PubMed]
6. Yıldız, T.C.; Freund, W.; Liu, J.; Schreck, M.; Khakhulin, D.; Yousef, H.; Milnea, C.; Grunert, J. Diamond sensors for hard X-ray energy and position resolving measurements at the European XFEL. *J. Synchrotron Rad.* **2024**, *31*, 1029–1036. [CrossRef] [PubMed]
7. Zhou, T.; Ding, W.; Gaowei, M.; De Geronimo, G.; Bohon, J.; Smedley, J.; Muller, E. Pixelated transmission-mode diamond X-ray detector. *J. Synchrotron Rad.* **2015**, *22*, 1396–1402. [CrossRef]
8. Claps, G.; Murtas, F.; Foggetta, L.; Di Giulio, C.; Alozy, J.; Cavoto, G. Diamondpix: A CVD diamond detector with timePix3 chip interface. *IEEE Trans. Nucl. Sci.* **2018**, *65*, 2743–2753. [CrossRef]
9. Griesmayer, E.; Kavrigin, P.; Weiss, C. The Use of Single Crystal CVD Diamond as Position Sensitive X-ray Detector. In Proceedings of the 5th International Beam Instrumentation Conference IBIC-2016, Barcelona, Spain, 11–15 September 2016; ISBN 978-3-95450-177-9.
10. Girolami, M.; Serpente, V.; Mastellone, M.; Tardocchi, M.; Rebai, M.; Xiu, Q.; Liu, J.; Sun, Z.; Zhao, Y.; Valentini, V.; et al. Self-powered solar-blind ultrafast UV-C diamond detectors with asymmetric Schottky contacts. *Carbon* **2022**, *189*, 27–36. [CrossRef]
11. Salvatori, S.; Girolami, M.; Oliva, P.; Conte, G.; Bolshakov, A.; Ralchenko, V.; Konov, V. Diamond device architectures for UV laser monitoring. *Laser Phys.* **2016**, *26*, 084005. [CrossRef]
12. Girolami, M.; Conte, G.; Salvatori, S.; Allegrini, P.; Bellucci, A.; Trucchi, D.M.; Ralchenko, V.G. Optimization of X-ray beam profilers based on CVD diamond detectors. *J. Instrum.* **2012**, *7*, C11005. [CrossRef]
13. Desjardins, K.; Bordessoule, M.; Pomorski, M. X-ray position-sensitive duo-lateral diamond detectors at SOLEIL. *J. Synchrotron Rad.* **2018**, *25*, 399–406. [CrossRef] [PubMed]
14. Saito, T.; Hayashi, K. Spectral responsivity measurements of photoconductive diamond detectors in the vacuum ultraviolet region distinguishing between internal photocurrent and photoemission current. *Appl. Phys. Lett.* **2005**, *86*, 122113. [CrossRef]
15. Ciancaglioni, I.; Marinelli, M.; Milani, E.; Prestopino, G.; Verona, C.; Verona-Rinati, G.; Angelone, M.; Pillon, M. Secondary electron emission in extreme-UV detectors: Application to diamond based devices. *J. Appl. Phys.* **2011**, *110*, 014501. [CrossRef]
16. Almaviva, S.; Marinelli, M.; Milani, E.; Prestopino, G.; Tucciarone, A.; Verona, C.; Verona-Rinati, G.; Angelone, M.; Pillon, M. Extreme UV photodetectors based on CVD single crystal diamond in a p-type/intrinsic/metal configuration. *Diam. Relat. Mater.* **2009**, *18*, 101–105. [CrossRef]

17. Angelone, M.; Pillon, M.; Marinelli, M.; Milani, E.; Prestopino, G.; Verona, C.; Verona-Rinati, G.; Coffey, I.; Murari, A.; Tartoni, N.; et al. Single crystal artificial diamond detectors for VUV and soft X-rays measurements on JET thermonuclear fusion plasma. *Nucl. Instrum. Methods Phys. Res.* **2010**, *A623*, 726–730. [CrossRef]
18. Prins, J.F. Preparation of ohmic contacts to semiconducting diamond. *J. Phys. D Appl. Phys.* **1989**, *22*, 1562–1564. [CrossRef]
19. Park, B.Y.; Zaouk, R.; Madou, M.J. Fabrication of Microelectrodes Using the Lift-Off Technique. In *Microfluidic Techniques*; Methods in Molecular Biology™; Minteer, S.D., Ed.; Humana Press: Totowa, NJ, USA, 2006; Volume 321. [CrossRef]
20. Ciancaglioni, I.; Di Venanzio, C.; Marinelli, M.; Milani, E.; Prestopino, G.; Verona, C.; Verona-Rinati, G.; Angelone, M.; Pillon, M.; Tartoni, N. Influence of the metallic contact in extreme-ultraviolet and soft x-ray diamond based Schottky photodiodes. *J. Appl. Phys.* **2011**, *110*, 054513. [CrossRef]
21. Available online: https://www.diamond.ac.uk/Science/Research/Optics/B16.html (accessed on 19 October 2025).